The Journal of the Society for Art and Science, Vol. 21, No. 3, pp. 136 – 145 (2022)

Evaluation Method for Shape Similarities between Archaeological Unorganized Point Cloud

Amartuvshin Renchin-ochir[1)], Zorig Badarch[1)], Kouichi Konno[2)]

[1)] School of Engineering and Applied Science,
National University of Mongolia, Ulaanbaatar, Mongolia
[2)] Graduate School of Science and Engineering, Iwate University, Iwate, Japan

amartuvshin@seas.num.edu.mn

Abstract
Researchers assume that the bodies of several Tara statues may have been molded from the same template. Therefore, researchers are eager to study the shape similarities between the Tara statues. Motivated by the archaeologist's requirements, this study presents an efficient approach to evaluate shape similarities between point clouds of two different Tara statues right-arm models. The evaluation approach consists of two main stages. The first is the reconstruction of individual body parts without decoration using a B-spline surface approximation technique. In previous reconstruction process, the surrounding surface selection parameter was manually specified. If the manually applied parameter is inadequate, it reduces the accuracy of the surface approximation and hole-filling, resulting in reduced accuracy of the evaluation result. Therefore, in this study, the surrounding surface selection parameter is automatically determined based on the Golden-section-search algorithm. The second stage evaluates the shape similarities between two different point clouds. The evaluation method considers a simple point-to-surface distance metric method with overlapping-surface detection and when compared with generic point-to-point distance metric method, the evaluation results proved that the proposed methodology was reliable and effective for this application. The approximation accuracy affects the evaluation result when the reconstruction method fills the gap by adding new points through the approximated surface. Therefore, in this study, the shape similarities were investigated between the two arm models with holes, immediately after separating the decoration parts.

1 Introduction

Mongolian government maintains remarkable cultural heritages of Tara statues. The great artist Zanabazar created those statues in the 17th-century, known as *"White Tara"*, *"Akshobhya"*, and *"Vairochana"* are shown in Figure 1.

Many artisans and archaeologists are keen to study sculptural techniques. They concurred under the assumption that the several parts of the Tara statues might be molded from the same template. To verify this assumption, they want to examine shape similarity between the body shapes of the Tara statues. However, this is a difficult with traditional archaeological devices. Furthermore, working on the Tara statues' original model is prohibited as the statues are under government protection. Fortunately, the Mongolian government has created a digitally scanned model of the Tara statues. Those digital models were constructed by the method presented in [1]. The authors measured statues from various angles to cover the whole surface with the "Konica Minolta vivid 9i" laser scanner in [1]. The scanning accuracy was 0.2 mm. Totally 235 scans were required to construct a complete White tara model with approximately

Figure 1: (a) White Tara, (b) Akshobhya and (c) Vairochana *(Gilt, bronze,* $68 \times 45 \times 45cm$*). (Photographs from "www.zanabazarfam.mn" and "www.zanabazar.com")*

29 million points. In the case of Akshobhya, the total number of scans was 194, and 225 scans were for Vairochana. The complete model of the Akshobhya contains approximately 19 million points and the Vairochana model contains approximately 20 million points. The scanning process took about two days per statues. Using those scanned models, it is possible to evaluate the shape similarities between body parts of the two statues.

As the statues contains various decorations on its body surface, it is difficult to evaluate the shape similarities. Therefore, in the previous study [2], we suggested the two methods: complex hole-filling and the point-cloud-based shape similarity evaluation method. In the complex hole-filling method, the surrounding surface selection parameter is specified manually. If the manually selected parameter is inadequate, it reduces the accuracy of the surface approximation and the hole-filling. Finding a sufficient surrounding surface selection parameter manually is very time consuming process. Therefore, the surrounding surface selection parameter is automatically determined based on the golden-section-search algorithm. The two arm parts that contain artificially generated points as hole-filling results were used in the previous evaluation. The evaluation result include the approximation error. Therefore, in this study, the shape similarity of two arm models were examined with the holes on the surface instead of artificially generated points to fill the holes.

2 Related works

Reconstruction of the individual, undecorated body parts: The first step was to detect decoration from the body using the point cloud model. The segmentation of decorated surfaces has rarely been studied [3, 4], and these methods cannot be applied to fine crafted decorative surfaces. The method of segmenting the decoration was developed in a previous study [5] with the decorations obtained from the shoulder and upper arm. This is followed by an unusual hole in the surface of the Tara statue's right hand. Several hole-filling algorithms have been suggested, including Guo Xiaoyuan's algorithm was for simple hole-filling [6] and Wang Jianning's algorithm [7] for complex holes with an island, covering only half of our problem, which consists of hole as well as gaps. Another study of hole-filling was suggested by Amitish [8], which can only fill simple holes on highly variable surfaces. A review of these related studies [6, 7, 8] showed that their methods need modification. Our suggested method is a uniform B-spline surface [9]. It is important to determine the exact area surrounding the hole. An improved version of the method [9] which automatically determines sufficient surrounding area, was used to reconstruct the holes and gaps of the model, in this article.

Evaluation of the shape similarity: Measuring similarity between 3D objects is widely used to measure the global similarity between two complete objects. However, only a few methods are proposed for measuring the similarity between 3D point clouds [10]. In point-cloud-based methods, accurate registration methods are widely used to create a complete model using separate point clouds captured by scanning devices from different points of view [11, 12, 13]. Existing registration algorithms can be classified into two types: pairwise registration and multi-view registration. Each of these method attempts to evaluate the optimal hard transformation, which maps the source point cloud to the target point cloud [13]. The most famous of them is the Iterative Closest

Point (ICP) algorithm and its variants based on iterative minimization of error metrics to estimate point correspondences between two or more point clouds [14]. The study [14] divided the ICP algorithm process into four steps: *Selection*, *Matching*, *Rejection*, and *Alignment*. When point clouds were aligned, the similarity between the two surfaces can be evaluated. In other words, the calculated distances between the corresponding regions of the surface may indicate the similarity of the shape between the clouds of points, as in the case of considering the similarities in the parts of the body of the statues of Tara. For example, a point-to-point error metric method was introduced, which uses the distance between the source point and the plane described by the target point and its local surface normal [11, 14, 15, 16]. Therefore, the generalized-ICP algorithm, which generalizes the metric of the point-to-point and point-to-plane errors, was introduced in [12].

With the advantage of the generalized-ICP method, our method implemented a simple and effective method for evaluating the similarity of shapes between two arm models of the Tara statues. However, another study [17] evaluated the point-to-point distance information, in which an attempt was made to assess the similarity between the two types of objects obtained by different data acquisition systems. Therefore, as part of this study, we also compared our implemented method with the point-to-point distance-based estimation method. However, the evaluation results include the approximation error. Therefore, in this study, we examined the shape similarity of the two arm models with holes on the surface instead of artificially generated points to fill the holes. The methods presented in this paper do not consider very complex parts, such as the crown on the head, earnings or faces, since they are completely different on all the statues.

3 Methodology

Archaeologists have focus on the arm models of the Tara statues because the arms look very similar. The experimental arm models have a bracelet and chain-shaped accessories on their surfaces, as shown in Figure 1. The general process flow of the reconstruction of the individual, undecorated body parts, and shape similarity evaluation process is summarized in Figure 2. The accessories in the sub-area of the target object have been referred to as *"decoration"* illustrated by the green shape in Figure 2, and the other body surfaces have been referred to as *"background"*. The input

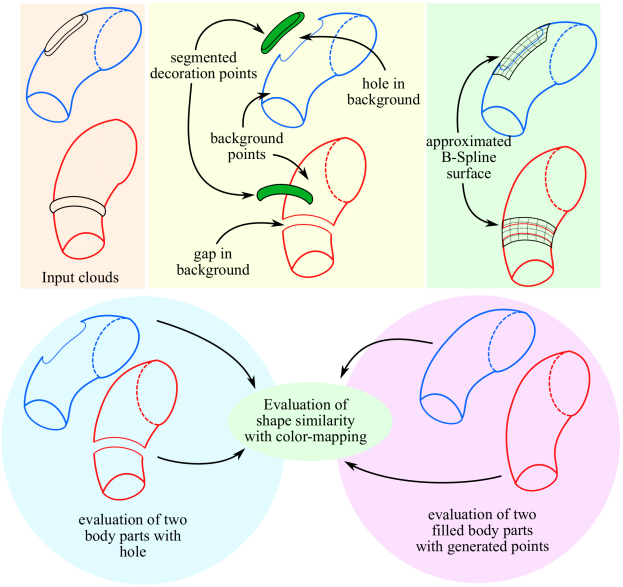

Figure 2: The process flow of the evaluation method.

point cloud of the arm model is separated into decoration and background point clouds using the segmentation method. After decoration and background parts were separated, large holes and gaps were appeared on the background; thus, the complex hole-filling method [9] based on B-spline surface fitting was used to restore a contiguous background surface. The proposed hole-filling methods were suitable to apply for three types of holes: a simple hole, a hole with an island and a gap separating the background into two surfaces.

A uniform B-spline surface with two topological parameters, u and v, in Figure 3, was used. First, regularly shaped either "*rectangular*" or "*cylindrical*" surfaces $\mathbf{S}_{i,j}$ which encircled the hole boundary, were defined as represented by the green and blue surfaces in Figure 3. A rectangular surface is shown in this

figure as an example.

When the outer area is defined, the following steps are completed in the method [9].

1. The outer area size was expanded by manually initialized parameter to obtain enough points around a target hole. The expanded outer area is illustrated in the green, blue, and red surfaces in Figure 3.

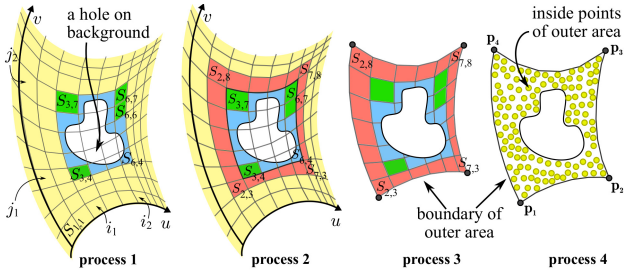

Figure 3: Process diagram of obtaining the inside points of the outer area.

2. The inside points of the outer area, as illustrated by the yellow points in Figure 3, were obtained from the background points set.

3. According to the obtained inside points, a cubic B-spline curve approximation, with knot insertion was then applied for every four boundaries, according to the instructions given in chapter 9 in [18].

4. The boundary curves were approximated again using the merged knot vectors, and then the new control points of the boundary curves were used as the outer control points of the B-spline surface.

5. Since the outer control points and knot vectors are known, the B-spline surface can be easily approximated using the least-squares approximation technique, which minimizes the average distance f derived by Eq. (1). Newton's method was used to calculate the normal vector between the B-spline surface and the corresponding points. The average distance f is referred to as precision. Where, $\mathbf{Q}_s (0 \leq s \leq t)$ denotes the inside points of the outer area, obtained by "*Step 2*". The number of the inside points $(t+1)$ depends on the outer area size. $\mathbf{S}(\overline{u}_s, \overline{v}_s)$ is the corresponding points on the approximated B-spline surface.

$$f = \frac{\sum_{s=0}^{t} |\mathbf{Q}_s - \mathbf{S}(\overline{u}_s, \overline{v}_s)|^2}{t+1} \tag{1}$$

When the outer areas are successfully approximated, locally uniform points inside the hole can be generated to complete the body surface. The standard deviation of the background point cloud was used to generate the local uniform points.

To ***determine a sufficient expanding parameter***, the parameter used to expand the outer area influences the accuracy of the surface approximation result. If the outer area is too small, the approximated B-spline surface might not efficiently be fitted on the surface around a hole. In contrast, if the outer area is too large, the number of the control points may be inadequate for approximation. Therefore, a sufficient expansion value should be considered for each hole. Hence, an improved version of the method [9] is presented and used in this study.

Let j be the expanding parameter of the outer area. In the example shown in Figure 3, the expanding parameter j is equal to 1. The golden-section search algorithm [19] is used to find the sufficient expanding value, according to the minimum precision of f, which variance depends on j. To find the local minimum, the golden-section search algorithm requires the searching interval, which is $1 \leq j \leq 20$ in our case. That interval was sufficiently wide to find the sufficient expanding parameter. For any j value, the precision f is calculated by steps 1 to 5 described above.

Once the arm parts from the different statues were available in an undecorated form, the body part shape similarity evaluation process could proceed on the complete body surface.

Evaluation of shape similarity: Archaeologists have been eager to examine similarities between Tara statues parts, as mentioned earlier, therefore, we developed a simple and efficient evaluation method in the previous study [2], which displays a color instead of the distance between two surfaces.

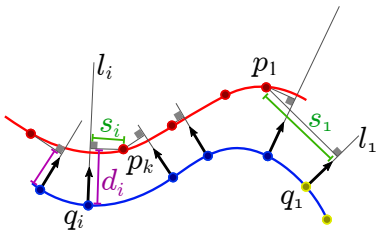

Figure 4: Overlapping distance calculations and restrictions.

In summary, our improved evaluation method was completed following these simple steps.

- The source and target clouds were aligned using the generalized-ICP algorithm proposed in [12]. The median of the two point clouds was used as the initial position for alignment.
- The distance between two surfaces was estimated using the point-to-plane distance metric in an overlapping region, which was derived using the method proposed in this section.
- The distance between two overlapped surfaces was visualized using the color according to the color mapping function.

The distance between two aligned surfaces of the arm models was derived using the improved point-to-plane error metric in the study [2]. The distance between two surfaces was derived from the distance between the source point, p_k, and the plane described by target point q_i and its local surface normal. The points p_k and q_i are the corresponding nearest neighbors. The two surfaces matched locally because the arm models were separated from different statues; therefore, some regions near the armpits have low density and might have been missed. For this reason, overlapping surfaces must be included when estimating shape similarity.

Let l_i be a line defined by the point q_i and its normal vector to the local surface normal. Then, the distance s_i between point p_k and l_i can be easily calculated. For example, distance s_1 between point p_1 and the line l_1 is shown in Figure 4, where if the distance $s_i \geq 3 \times s_P$, point q_i must be dealt with in a non-overlapping surface. Where s_P is the standard deviation of the P point cloud distribution, and the multiplier "3" was determined by our experience, according to the normal distribution of the standard deviation.

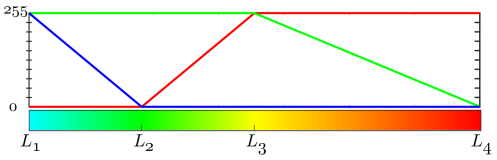

Figure 5: The color mapping used to visualize distance.

Once, the overlapping surface has been determined, the distance d_i between overlapping surfaces can be visualized with a color mapping, which was formulated using Eq. (2).

$$f(d_i) = \begin{cases} \left(0, 255, 255 \cdot (1 - \frac{d_i - L_1}{L_2 - L_1})\right), & \text{if } L_1 \leq d_i < L_2 \\ \left(255 \cdot \frac{d_i - L_2}{L_3 - L_2}, 255, 0\right), & \text{if } L_2 \leq d_i < L_3 \\ \left(255, 255 \cdot (1 - \frac{d_i - L_3}{L_4 - L_3}), 0\right), & \text{if } L_3 \leq d_i \leq L_4 \end{cases} \quad (2)$$

Where the $d_i (1 \leq i \leq n)$ is the distance, $L_1 = \min(d_i)$ is the minimum, $L_4 = \max(d_i)$ is the maximum, and $L_2 = \bar{d}_i$ is the mean of the d_i. Furthermore, another distance level, L_3, is equal to $L_2 + (L_2 - L_1)$. The color mapping function and RGB vectors are shown in Figure 5.

The comparison between our implemented evaluation method and the distance between two surfaces estimated by the point-to-point distance metric is presented in the following Section.

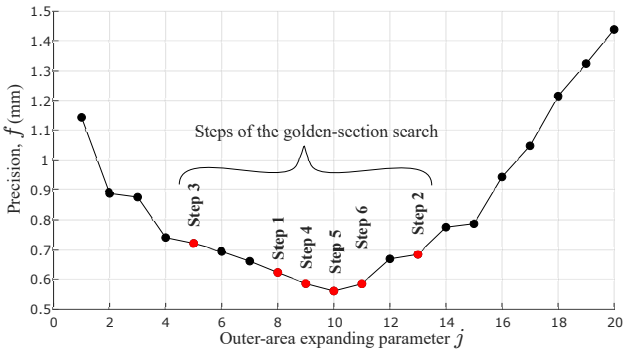

Figure 6: Graph of precision, f for each expanding parameter j.

4 Experimental results

The constructed Buddha models contain many

decorations covering the whole body. According to the archaeologists' interest, we focus on the body parts which might be molded from the same template except for parts like the head, face and throne in this experimental result. Because those parts are the special feature of each statue. Since segmentation and hole-filling algorithms used in our study are applicable on cylindrically shaped manifold surfaces, it is possible to verify the reliability of our methods on a few parts of the buddha models such as the arm and chest. The arm parts of each buddha seem more similar compared to the chest, then, we consider the arm parts in this study.

The graph of precision f is created for each expanding parameter j to confirm the efficiency of the improved method, as shown in Figure 6. The vertical axis indicates the precision, f, derived by the Eq. (1) for the expanding parameter $j \in [1, 2, ..., 20]$ on the horizontal axis. A sufficient expanding value was found by the golden-section search algorithm at the 6th step of the iteration. In the first step, j was 8, and then 13, 5, 9, 10, and 11, according to the result of the golden-section algorithm shown in Figure 6. The sufficient expanding value was 10 and the minimum precision was approximately 0.56 mm.

For the shoulder shown in Figure 7 (a), the outer area shape was rectangular. For the upper-arm, the precision was approximately 0.24 mm, and the outer area shape was cylindrical. The generated points were uniformly distributed, and the maximum number of control points was "7" in both parametric directions of the fitted B-spline surface, according to the results from the knot insertion algorithm.

White Tara and *Akshobhya* statue arm models were reconstructed with automatically determined parameters using the improved method. The solid models of experimental models are shown in Figure 7 for clear visualization. However, the surface fitting approximation was better than the previous result presented in the study [9]. The precision of the approximated surfaces generated using the previous method and improved method has been summarized in Table 1.

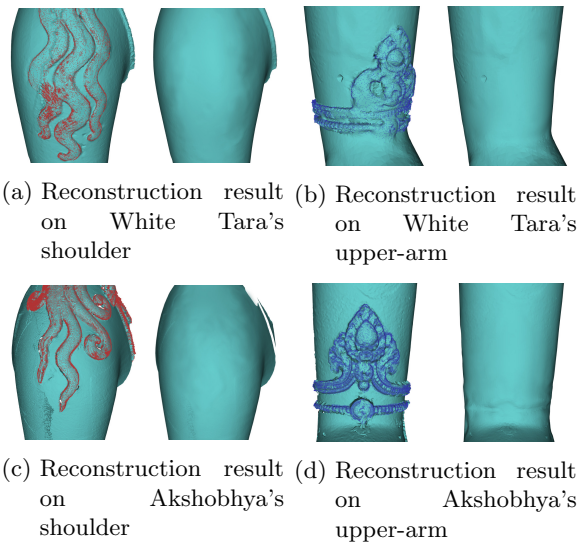

(a) Reconstruction result on White Tara's shoulder (b) Reconstruction result on White Tara's upper-arm

(c) Reconstruction result on Akshobhya's shoulder (d) Reconstruction result on Akshobhya's upper-arm

Figure 7: Solid models showing original surface with decoration and its reconstructed body surfaces.

Table 1: precision of the approximated surfaces

Approximated surfaces	precision (mm) method [9]	our method
White Tara's shoulder	0.73	0.56
White Tara's upper arm	0.48	0.24
Akshobhya's shoulder	0.70	0.54
Akshobhya's upper arm	0.28	0.28

4.1 Evaluation of the shape similarity

The reconstruction results made it possible to evaluate the similarity of the arm models. A summary of the two reconstructed point clouds has been presented in Table 2. The density of the Akshobhya's arm model was much higher than White Tara's arm model, according to the standard deviation. As mentioned earlier, the scanned point cloud was registered from the multiple views. Therefore, some surfaces have a higher density, depending on the view points used to reconstruct the surface. White Tara's arm model was nominated as the source cloud and Akshobhya's arm model was referred to as the target cloud. The results of the generalized-ICP

Table 2: Statistics of the input point clouds for evaluation

input cloud	points	standard deviation(mm)
White Tara's arm	59392	1.04
Akshobhya's arm	317971	0.016

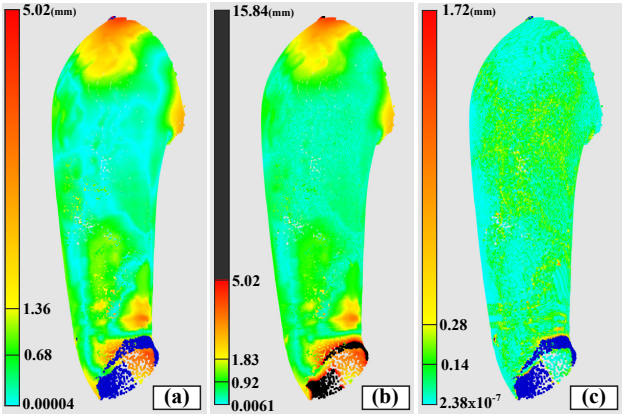

Figure 8: (a) Color mapping distance results after applying our implemented method, (b) distances calculated by point-to-point error metric, and (c) differences between the distances portrayed by (a) and (b).

algorithm were completed after 50 iterations, and the convergence rate was approximately 1.89 mm. In this experiment, a low convergence rate is expected as two models belonged to different statues.

The result of the implemented color mapping is shown in Figure 8 (a), where distances between the two surfaces were derived using the point-to-plane error metric. Then, the color mapping is applied to the overlapped surfaces where the blue points represent the non-overlapping surfaces. The minimum distance between the two surfaces was approximately 0.04×10^{-3} mm, and has been illustrated by the cyan color. The mean distance was approximately 0.68 mm and is illustrated by the green color. The vertical color bar shows color mapping representation of distance in which the distance from 1.36 to 5.02 mm is represented by yellow to red color.

We applied the same color mapping to the distance between two surfaces is derived by point-to-point error metric without considering overlapping regions. However, the distance greater than 5.02 mm was represented by black. The results are presented in Figure 8 (b). The maximum distance was approximately 15.84 mm. If the non-overlapped surface regions were larger, the maximum distance would have been shown to be greater using the point-to-point error metric; as this was not the case, it is evident that our improved evaluation method was able to visually represent the distance precisely.

Next, the difference between the distances calculated using our method and the point-to-point error metric was calculated and illustrated using color mapping, as shown in Figure 8 (c). The minimum difference was approximately 2.38×10^{-7} mm, and the maximum was 1.72 mm around the boundary of the surfaces as illustrated by red color in Figure 8 (c). The point cloud density differences contributed to these differences.

The evaluation result in Figure 8 includes the result of the approximation error, especially around location where once decoration existed. Therefore, we examine the similarity between the arm models with holes on the surface instead of artificially generated points to fill the holes. The evaluation result is presented in Figure 9.

The maximum distance between two surfaces, calculated by our proposed method in Figure 9 (a) was smaller than that shown in Figure 8 (a). However, the maximum distance between two surfaces calculated by the point-to-point error metric in Figure 9 (b) was larger than the maximum distance shown in Figure 8 (b). This is because the two models had large holes and had larger non-overlapping surfaces. Therefore, our proposed evaluation method is robust for non-overlapping surfaces. The differences between the distances calculated using our method and the point-to-point error metric were illustrated using color mapping shown in Figure 9 (c).

Figure 10 shows histograms of the distance estimated by our work and by the point-to-point error metric. The horizontal axis indicates

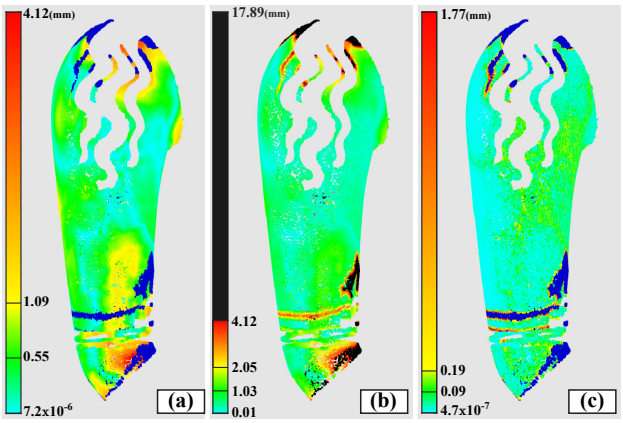

Figure 9: (a) Color mapping distance results after applying our implemented method, (b) distances calculated by point-to-point error metric, and (c) differences between the distances portrayed by (a) and (b).

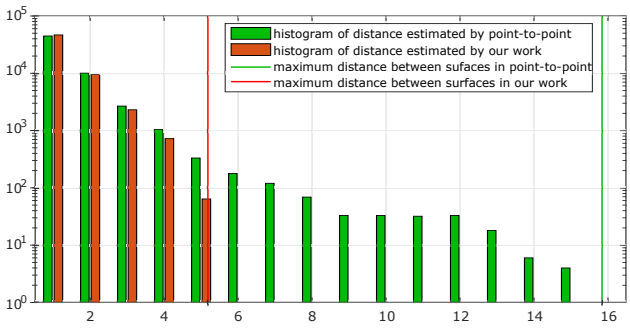

Figure 10: Histograms showing distances estimated using our method and using point-to-point error metric.

distance information (mm), while the vertical axis is logarithmic.

The histogram indicates that the distribution estimated by our method was narrower, and thus, considering the color bars in Figure 8 and the histogram in Figure 10, we were able to conclude that our evaluation method, as implemented here, can precisely illustrate the distance.

In summary, the efficiency of the point-to-plane error metric was compared with a point-to-point error metric, and according to the color mapping outcomes, the results were very similar, as shown by the amount of the cyan and green coloring in Figure 8 (a). Hole-filling is error prone as it influences the shape similarity; undecorated arm models were created to reduce this error evaluation, as in Figure 9 (a). The average distance between the two hole-filled surfaces was less than 0.68 mm, and in the undecorated arm model was 0.55 mm which is the most important factor for archaeologists to verify their assumption.

5 Conclusions

In this study, we improved the hole-filling method using the Golden-section-search and made shape similarity on two undecorated arm models for better evaluation. Undecorated complete arm models were reconstructed using the improved hole-filling method, which helped to achieve good results to evaluate shape similarity. Therefore, archaeologists can use it per their requirements: the method allows them to easily analyze the Tara statue's body shape similarities, based on the surface differences. We will use feedback from archaeologists to improve this evaluation method, and will test the methodology on the other parts of the Buddha statues, such as the chest and elsewhere, in future.

Acknowledgment

The author would like to thank the MJEED JR14B16 project for financial support.

References

[1] B. Tsendsuren, O. Khorloo, and E. Altantsetseg, "Point cloud processing for constructing 3d models," *Management Innovation Scientific Journal*, vol. 1, pp. 307–311, 2016.

[2] A. Renchin-ochir, E. Altantsetseg, and K. Konno, "A study of analyzing shape similarities between the arm model of mongolian buddha statues for archaeological applications," in *2019 International Conference on Cyberworlds (CW)*, Oct 2019, pp. 387–390.

[3] M. Weinmann, A. Schmidt, C. Mallet, S. Hinz, F. Rottensteiner, and B. Jutzi,

"Contextual classification of point cloud data by exploiting individual 3d neighbourhoods," *ISPRS annals of the photogrammetry, remote sensing and spatial information sciences*, vol. 2, no. 3, p. 271, 2015.

[4] X. Chen, A. Golovinskiy, and T. Funkhouser, "A benchmark for 3d mesh segmentation," in *ACM SIGGRAPH 2009 Papers*, ser. SIGGRAPH '09. New York, NY, USA: ACM, 2009, pp. 73:1–73:12. [Online]. Available: http://doi.acm.org/10.1145/1576246.1531379

[5] A. Renchin-Ochir, K. Matsuyama, E. Altantsetseg, and K. Konno, "A segmentation algorithm for decoration on arm part of mongolian buddha statue based on medial axis," in *NICOGRAPH 2017*. The Society for Art and Science, 2017, pp. 25–32.

[6] X. Guo, J. Xiao, and Y. Wang, "A survey on algorithms of hole filling in 3d surface reconstruction," *The Visual Computer*, vol. 34, no. 1, pp. 93–103, 2018.

[7] J. Wang and M. M. Oliveira, "Filling holes on locally smooth surfaces reconstructed from point clouds," *Image and Vision Computing*, vol. 25, no. 1, pp. 103–113, 2007.

[8] A. Kumar, A. Shih, Y. Ito, D. Ross, and B. Soni, "A hole-filling algorithm using non-uniform rational b-splines," in *Proceedings of the 16th International Meshing Roundtable*, 2008, pp. 169–182.

[9] A. Renchin-Ochir, E. Altantsetseg, and K. Konno, "Hole-filling method for reconstructing separated arm models of the mongolian buddha statue for analyzing body shape of statues," in *Proceedings of the 16th ACM SIGGRAPH International Conference on Virtual-Reality Continuum and its Applications in Industry*. ACM, 2018, pp. 28:1–28:8.

[10] Z. Zhanga, J. Lia, X. Lic, Y. Lina, S. Zhanga, and C. Wanga, "A fast method for measuring the similarity between 3d model and 3d point cloud," *International Archives of the Photogrammetry, Remote Sensing and Spatial Information Sciences*, vol. 1, 2016.

[11] Y. Chen and G. Medioni, "Object modeling by registration of multiple range images," *Image and vision computing*, vol. 10, no. 3, pp. 145–155, 1992.

[12] A. Segal, D. Haehnel, and S. Thrun, "Generalized-icp." in *Robotics: science and systems*, vol. 2, no. 4, 2009, pp. 435–442.

[13] B. Bellekens, V. Spruyt, R. Berkvens, and M. Weyn, "A survey of rigid 3d pointcloud registration algorithms," in *AMBIENT 2014: the Fourth International Conference on Ambient Computing, Applications, Services and Technologies, August 24-28, 2014, Rome, Italy*, 2014, pp. 8–13.

[14] D. Holz, A. E. Ichim, F. Tombari, R. B. Rusu, and S. Behnke, "Registration with the point cloud library: A modular framework for aligning in 3-d," *IEEE Robotics & Automation Magazine*, vol. 22, no. 4, pp. 110–124, 2015.

[15] A. W. Fitzgibbon, "Robust registration of 2d and 3d point sets," *Image and Vision Computing*, vol. 21, no. 13, pp. 1145–1153, 2003.

[16] K.-L. Low, "Linear least-squares optimization for point-to-plane icp surface registration," *Chapel Hill, University of North Carolina*, vol. 4, no. 10, 2004.

[17] P. Grussenmeyer, T. Landes, T. Voegtle, and K. Ringle, "Comparison methods of terrestrial laser scanning, photogrammetry and tachometer data for recording of cultural heritage buildings," *International Archives of Photogrammetry, Remote Sensing and Spatial Information Sciences*, vol. 37, no. B5, pp. 213–218, 2008.

[18] L. Piegl and W. Tiller, *The NURBS Book*, ser. Monographs in Visual Communication. Springer Berlin Heidelberg, 1996.

[19] R. P. Brent, *Algorithms for minimization without derivatives*. Courier Corporation, 2013.

Amartuvshin Renchin-Ochir

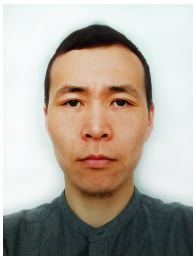

Amartuvshin Renchin-Ochir is an associate professor at National University of Mongolia. He received the B.Sc. and M.E. degrees from the National University of Mongolia in 2007 and 2010. He earned his Dr. Eng. in Design and Media technology from Graduate School of Engineering from Iwate University in 2019. He worked on a lecturer of School of Engineering and Applied Sciences at National University of Mongolia from 2012 to 2016. His research interests include point cloud processing, geometric modeling, computer graphics, computer vision and robotics.

Zorig Badarch

Badarch Zorig received the B.Sc. and M.E. degrees from the Mongolian University of Science and Technology in 2004 and 2007. He worked as a lecturer School of Engineering and Applied Sciences at the National University of Mongolia from 2012 till now. His research interests include geometric modeling, computer vision, and automation.

Kouichi Konno

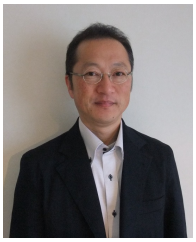

Kouichi Konno is a professor of Faculty of Engineering at Iwate University. He received a BS in Information Science in 1985 from the University of Tsukuba. He earned his Dr.Eng. in precision machinery engineering from the University of Tokyo in 1996. He joined the solid modeling project at RICOH from 1985 to 1999, and the XVL project at Lattice Technology in 2000. He worked on an associate professor of Faculty of Engineering at Iwate University from 2001 to 2009. His research interests include virtual reality, geometric modeling, 3D measurement systems, and computer graphics. He is a member of EuroGraphics.